CHAPTER 3

InGaN Quantum Dots Grown on SiN Nanoholes

3.1 Introduction

The related III-V nitride materials with quantum confined structures were the most extensively investigated and would be used for the promising optical devices in the next generation, especially for light emitting diodes (LEDs) and laser diodes (LDs). However, the quantum confined effects causing by low-dimensional structure would bring the devices more effective properties such as operating in low threshold current, higher direct modulation speed, and reducing the temperature sensitivity.

Different dimension of structure has its own density of states, which including three-dimensional (3-D) structure of bulk material, 2-D structure of quantum well, 1-D structure of nanowire/ nanorod/ nanopillar, and 0-D structure of quantum dot (QD), shown in Fig. 3.1. A 3-D system has the parabolic-like density of states. For the 2-D structure, the density of state is made up of a pile of step functions. The density of states in a 1-D structure diverges at E_n and δ–function shape for the 0-D structure.

Within the last decade, there has been a lot of research devoted to the realization of the predicted behavior of 3-D quantum-confined structures. In 1982, the first concept of the QDs was proposed as artificial atoms for semiconductor laser applications by Arakawa and Sakaki [1]. The semiconductor laser with a QD active region they proposed promises many profound effects on various improvement, including ultra-low and temperature independent threshold current [1,2], high-frequency modulation with negligible chirping effect [3], high-temperature operation, and nonlinear gain effect [4]. By the end of the 1980s, the fabrication of QDs by lithographic patterning and etched QW structure was considered as the main techniques to fabricate QDs.

The crystal growth on a bulk substrate occurs in one of three distinct modes, Frank-van der Merwe (FM), Volmer-Weber (VW), and Stranski–Krastanow (SK). While growth proceeds layer by layer in the FM mode, VW growth causes three-dimensional islands on the substrate, if the film has a higher surface energy than that of the substrate. SK growth is a combination of the FM and VW modes, where the growth of a several-monolayer thin film, called a wetting layer, is followed by cluster nucleation and then to island formation. SK growth mode is formed with the strain-driven process when the misfit is larger than 1.7% [5]. Self-assembling growth is a convenient method to obtain QDs because not needs any

patterning process. In contrast, the position of the QDs is randomly distributed. Therefore, selective growth is used to control the position of QDs. Figure 3.2 shows a brief history of research on QD lasers particularly at the initial stage until 1999 [5].

There are several main growth methods to formed QD structure including S-K growth mode, antisurfactant growth method, and selective growth method. They are summarized below:

(I) S-K growth mode (layer-then-island)

The evolution of an initially of 2-D growth in to the front of a 3-D growth is a well-known phenomenon and has been frequently observed in various systems. This growth mode is used by various materials grown under compressive stress on hetero-structure by strain-driven quantum dot formation during hetero-epitaxy as a bottom-up approach. After the deposition of a few 2-D monolayers (MLs), island structures are self-formed on the 2-D wetting layer as a result of the transition of the growth mode and the stress induced by the lattices mismatch between the interfaces needs to be released, as shown in Fig. 3.3. The strain relaxation mechanisms would be first published by Stranski and Krastanow and we called the growth mode as S-K growth mode. Especially, the growth of self-assembled quantum dots (SAQD) on large area substrate with a good throughput and compatibility by the S-K growth mode has been successfully demonstrated for current microelectronic technology [15].

(II) Antisurfactant method

The phenomenon was observed and studied on Ge/Si systems, the surfactants such as As, Sb, or Sn can be used to suppress the formation of island structure [13, 15, 18]. We can use the unequal equation to show the surface free energy in 3-D growth mode in a system,

$$\delta_s < \delta_f + \delta_i \,,$$

where δ_s is the surface free energies of substrate, δ_f shows the surface free energies of film, and δ_i represents the surface free energies of interface between substrate and film. As a third element like the surfactant is added, the sign of the unequal equation would be change by altering the substrate surface free energy [16]. Using this growth method, the surfactant is believed to play an important role in changing the surface free energy of the material.

Some reports have shown reversed effect occurs in GaN-based system [16, 17]. The antisurfactant is believed to inhibit the film growth and intentionally modify the 2-D mode into 3-D mode. However, the role of the antisurfactant is still unknown in the enhancement of island growth, Therefore, carrying out the basic mechanism in growth way would be important to us for further studies in detail. This chapter would focus on the growth of antisurfactant method using the SiN as an antisurfactant. This is different from many other

groups.

(III) Selective method

Self-assembling growth is a convenient growth method of QDs but the position of the QDs is difficult to be controlled. Using selective method to obtain QDs, in the contrast, the shape, size, and position of the QDs could be artificially designed and controlled. In general, the selective method can control the position of the QDs by the methods of focused ion-beam irradiation and photo-assisted wet chemical etching. S. Sakai, *et al.* [18] grew the QDs on Si-patterned GaN/sapphire substrates. Different shapes QDs could be grown by using different patterns or masks. Here, we simply introduce the formation of InGaN QDs by selective method published by Y. Arakawa, *et al.* [5]. Figure 3.4 shows a scanning electrical microscope (SEM) bird's-eye-view and a cross-sectional view of InGaN QD structures. Shown in Fig. 3.4 (b), no material was deposited on the SiO_2 mask and the positions of the QDs were controlled very well.

In a quantum dot, the electronic states are quantized and the energy levels become discreted. In Fig. 3.5, we can see the carriers are localized in the quantum dot structure for 3-D confinement. Because of the localization of carriers trapped at QDs, in the strong confinement regime, i.e., in small size QDs, where the sub-band energy separations are much larger than the electron-hole Coulomb interaction of the exciton binding energy, the exciton ground state is mainly composed of the lowest-energy sub-band [15]. Finally, in the week-confinement regime where the quantum dot size is much larger than the exciton Bohr radius, the quantized sub-bands are distributed almost continuously and the binding energy is nearly the same as in the bulk material.

3.2 Experiment setup and sample preparation

(I) Photoluminescence measurement Setup

Photoluminescence (PL) is the optical emission obtained by photon excitation (usually a laser) and is commonly observed with III-V semiconductor materials. This type of analysis allows non-destructive characterization of semiconductors (material composition, qualitative investigations, etc. The PL spectra allow us to realize the radiative recombination process in the materials. Feature of the emission spectrum can be used to determine electronic energy level, such as identify surface, interface, and impurity levels and to gauge alloy disorder and interface roughness. The intensity of the PL signal provides information on the quality of surfaces and interfaces. Variation of the PL intensity with external parameters like temperature and applied voltage can be used to characterize further the underlying electronic states and

bands.

PL measurement system is shown in Fig 3.6. The excitation source was a non polarized and multi-mode Melles Griot Helium-Cadmium laser operated at 325 nm of 30 mW. After reflecting by three mirrors, the laser was focused by a lens, which focal length was 5 cm with 300 μm in diameter and the luminescence light was collected by the same lens. The luminescence light was dispersed by 0.32 m monochromator (Jobin-Yvon Triax-320) equipped with 300, 1200 and 1800 grooves/cm grating and the maximum width of the entrance slit is 1 mm.

300 grooves/cm grating and 0.1 mm slit was performed in my experiment. Under this condition, the wavelength resolution was approximately 1 nm. In order to prevent the spray laser light from the sample surface enters the detector, a long pass filter with a cut-off wavelength at 360 nm in front of the entrance slit is used. Finally, the collected luminescence light was detected by the charge coupled device (CCD).

(II) Photoluminescence excitation measurement

In PL measurement, which is performed at fixed excitation energy, the luminescence properties are generally investigated. While PL excitation (PLE) spectroscopy, which is carried out at fixed detection energy, provides mainly information about the absorption properties. Apart from absorption and PL experiments, the PLE measurement is a widely used spectroscopic tool for the characterization of optical transitions in semiconductors.

It is also very important to note that the PLE also depends strongly on the different carrier relaxation processes that connect the absorbing state to the luminescent state. For example, it is possible to recognize the absorption in a quantum well (QW) from that of the substrate if they have different emission energies, in which because it can be assumed that carrier transfer between substrate and QW is negligible. Nevertheless, in many cases it is difficult to separate the influence of relaxation from that of absorption. The PLE spectrum is strongly influenced by the relaxation depending on different samples.

Except for the excited source, the light collection system and spectrometer (Jobin-Yvon Triax-320) are the same as the PL system. As shown in Fig 3.7, the sample was mounted in the low temperature vacuum chamber and cooled down to 15K. The pumping source was Xe lamp with 300 W dispersed by double-grating monochromator (Jobin-Yvon Gemini 180) and then focused to the sample by two lenses. And then the signal was collected by PL system. The detector was a high sensitive Hamamatsu photomultiplier tube (PMT) with GaAs photocathode.

(III) Sample preparation

Three InGaN QDs samples that had undergone different durations of SiNx treatment of the underlying GaN layer before the InGaN layer was deposited, were grown on c-face sapphire substrates by metalorganic vapor phase epitaxy (MOVPE) [9-11]. A 30-nm-thick low-temperature GaN nucleation layer was first grown at $550^{o}C$. Then, the reactor temperature was increased to $1000^{o}C$ to grow a 2-µm-thick underlying Si- doped GaN underlying layer, providing a step-flow grown surface as confirmed by atomic force microscopy (AFM). Then, a rough SiN_x layer with varying thickness (or different durations of SiN_x treatment) was grown on the n-type GaN underlying layer. During the treatment of the SiN_x layer, the flow rates of NH_3 and the diluted Si_2H_6 were 5 slm and 50 sccm, respectively. The temperature was then ramped down to $800^{o}C$ to grow the $In_xGa_{1-x}N$ layers. As soon as the InGaN layers deposition completed, the growth temperature was reduced to room temperature (RT). During the growth of the InGaN layers, the vapor phase ratio TMIn/ (TMIn+TEGa) was fixed at 0.35. Additional InGaN layers capped with a 10 nm un-doped GaN layer, were grown to investigate the optical property of the InGaN layers. The detailed growth conditions of InGaN samples that had undergone various durations of SiN_x treatment of the GaN were examined, as listed in table 3.1. The optical characteristics of these three epitaxial samples were evaluated using RT-PL with a low 5mW He-Cd laser operated at 325 nm. The surface morphology of all samples grown was characterized by AFM. Scans were performed over a surface area of 500 nm, using a Digital Instruments Nanoscope with a sharpened Si_3N_4 tip. Figure 3.8 shows AFM images of the surface morphology of the samples QD-200, QD-240 and QD-315, respectively. Scans were performed over a surface area of 1 µm × 1 µm. The average lateral size and height of QD-200 are estimated to be about 33.2 nm and 0.64 nm. As increasing the duration of treatment, the QD sizes become larger, 35.2 nm of lateral size and 0.79 nm of height for sample QD-240. For sample QD-315, the average height is up to 2.4 nm and the lateral size is about 35.7 nm. The densities of the InGaN QDs were estimated to be increased approximately from 2.1×10^{11} cm^{-2} to 2.9×10^{11} cm^{-2} for these samples.

3.3 Optical Properties of the InGaN QDs

Figure 3.9 shows the corresponding normalized PL spectra for samples QD-200, QD-240 and QD-315 measured at room temperature. The dominant peak wavelengths for each spectrum are 428 nm, 433 nm and 448 nm, respectively, which clearly show a red-shift with the duration of SiN_x treatment. As listed in table 3.1, the average heights of the InGaN nano-islands and QDs were approximately estimated from the increase in AFM from 0.64 nm

to 2.4 nm as the duration of the SiN_x treatment increased from 120 to 195 sec. The redshift as the duration of the SiNx treatment increased could be attributed to the increasing height of the QDs (or nano-islands) due to quantum effects. Thus the red-shift in emission wavelength could be attributed to the changing in size or shape of the InGaN QDs [19].

The PL peak shift energy which is relative to that at 10K under different temperature for the three samples is showed in Fig. 3.10. For QD-200 and QD-240, the total shifts of around 10 meV were observed in the temperature range of 10-300K, and these shifts are obviously lower than that of bulk GaN (80 meV) [20] and InGaN/GaN MQW (54 meV) [19, 20]. In addition, we can use the Varshni equation to fit the curve of QD-315 in Fig. 3.10.

$$Eg(T) = Eg(0) - \frac{\alpha T^2}{\beta + T} \qquad \text{Eq. (3.1)}$$

It is well known that the red-shift of the band-gap energy originates from the interaction with phonon. The smaller red-shift observed for QD structures can be explained by partial decoupling of the phonon-exciton interaction of the QDs [22, 23]. The phonon coupling clearly decreases with QD size decreasing. Therefore, a direct consequence of the decreased phonon coupling is the smaller red-shift of the PL peak with increasing temperature [20]. Besides, the emission peaks of samples of QD-200 and QD-240 showed clearly the "S-shaped" (blue-red-blue) behavior below 200K. This could be explained by a carrier localization effect at low temperature. The blue-shift results from the confinement-induced shift of the electronic levels, whereas the red-shift results from the increased Coulomb energy induced by a compression of the exciton Bohr radius. In alloy In-homogeneity and/or In phase separation have been proposed as the origin of the localized states [24]. It reveals different potential fluctuations within these two samples compared with a larger size of high-density QDs.

3.4 Thermal Annealing Effects on Optical Properties of the InGaN QDs

There are several approaches to control the emission wavelengths of QDs, such as adjusting the sizes of QDs [19], changing the composition of dots/barrier [25], and thermal annealing [26]. For InGaAs/GaAs QDs, the effects of thermal annealing on their optical properties were studied and a blueshift in PL peak position was observed from the annealed QDs [27, 28]. The PL blueshift phenomenon was attributed to the inter-diffusion between the QDs and the barrier. However, there are only a few reports on the optical properties of thermal annealed InGaN QDs. In this report, the effects of thermal annealing on optical properties of the InGaN QDs grown by metalorganic chemical vapor deposition (MOCVD) were examined

using temperature-dependent PL measurements.

Here, the InGaN QDs samples of QD-200 were used for thermal annealing. There are three set of samples for measurements with different conditions. Samples A are the as-grown samples for comparison without further annealing. Samples B and C were thermal annealed at 850°C and 950°C, respectively, for 150s in nitrogen ambiance by rapid thermal annealing (RTA) and compared with the samples A. The PL spectra from these three samples are shown in Fig. 3.12. The emission peak energy of samples A, B, and C is at 2.81, 2.83, and 2.87 eV, which shows a blue-shift of PL peak positions with post-thermal annealing. For InGaAs/GaAs QDs, many reports have showed that RTA induces the In /Ga inter-diffusion, thus having the effect of blue-shifting on the PL emission energy, and decreasing of the barrier height [29]. On the other hand, the phase transformation of the inter-diffusion from the product phases of lower indium contents to the parent phases occurs as high indium-content InGaN/GaN quantum wells were post-grown annealed on different temperatures [30]. Thus, the blushifts of PL peak positions shown in Fig. 3.12 may be due to the changes in InGaN QDs shapes or sizes caused by the thermal annealing process [28].

In order to further investigate the optical properties of InGaN QDs after RTA process, the temperature-dependent PL measurements from 10K to 300K were performed. Figure 3.13 plots normalized PL intensity as a function of temperature for samples A, B, and C. The thermal activation energy, Ea, were estimated to be about 60, 55, and 41 meV by the fitting results based on the band tail model suggested by Eliseev et al. as follow [31],

$$\frac{I}{I_0} = \frac{1}{1 + A\exp(-\frac{E_a}{kT})}$$

Eq. (3.2)

The decrease in E_a of the annealed InGaN QDs can be interpreted as a decrease in the potential difference of barrier height and the shape of the confining potential caused by inter-diffusion during annealing progress. The similar results were also observed on InGaAs/GaAs and CdTe QDs system [24,28,32]. The annealing temperature, PL peak, blueshift, and activation energy of the three samples are summarized in table 3.1. It is clear that the thermal-annealing induced blue-shifts on the PL peaks of the InGaN QDs will accompany a decrease on their activation energy. Additionally, we found that thermal annealing at 950°C led to a blueshift of 57 meV and a decrease in thermal activation energy of about 19 meV.

In summary, we have studied the effects of thermal annealing effects on optical properties of the InGaN QDs grown on SiN nanohole. About 57 meV blueshifts of the PL

peak positions and a decrease on the activation energy of 19 meV were observed from the InGaN QDs after 950$^{\text{o}}$C annealing, which may be due to In /Ga inter-diffusion and variation on the QDs size by post-grown thermal annealing.

Table 3.1. Summary of growth condition, PL peak energy and QDs height for InGaN QDs.

Sample NO.	SiNx treatment time (min)	Peak energy (eV)	QDs height (nm)
QD-200	2	2.897	0.64
QD-240	2'40"	2.863	0.79
QD-315	3'15"	2.768	2.46
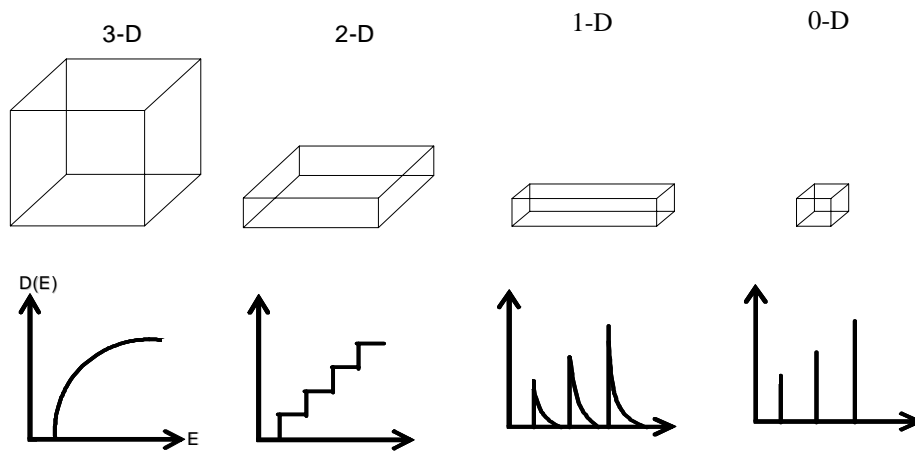
Fig. 3.1. The relation between dimension and density of states.
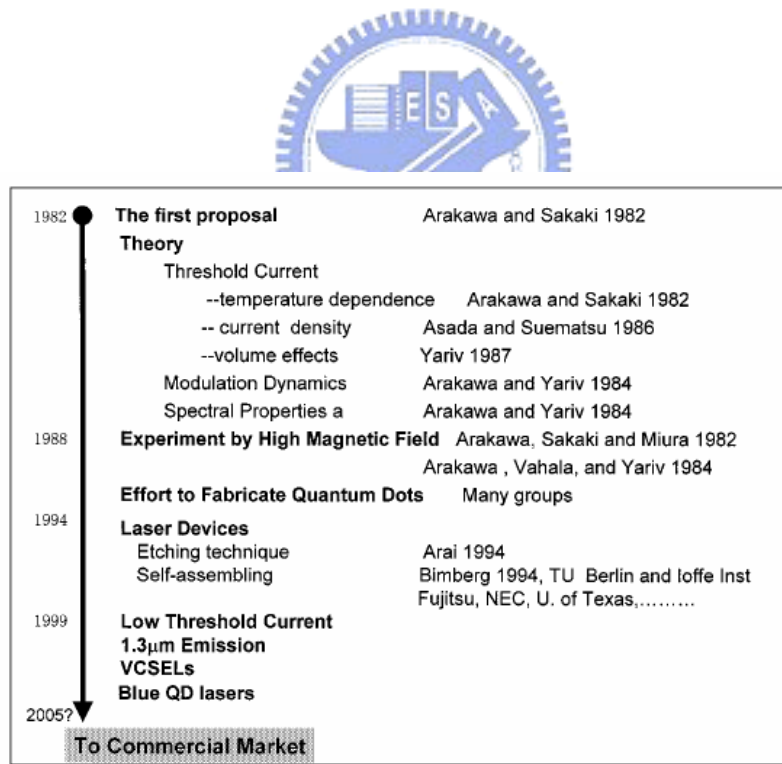
Fig. 3.2. A brief history of research on QD lasers particularly at the initial stage.
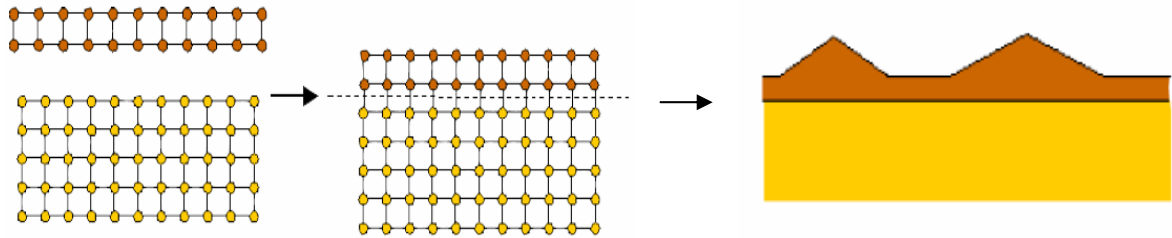
Fig. 3.3.   A diagram of strain relaxation for S-K growth mode.
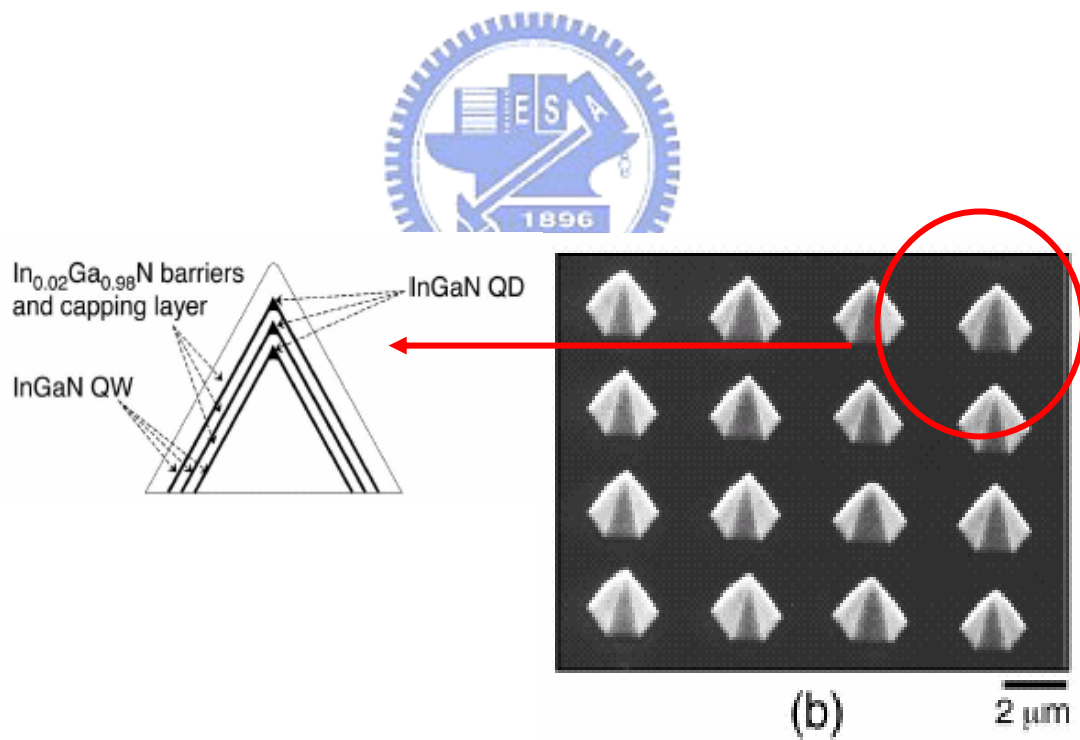
Fig. 3.4.   A SEM bird's-eye-view and cross-sectional view of InGaN QD structures.
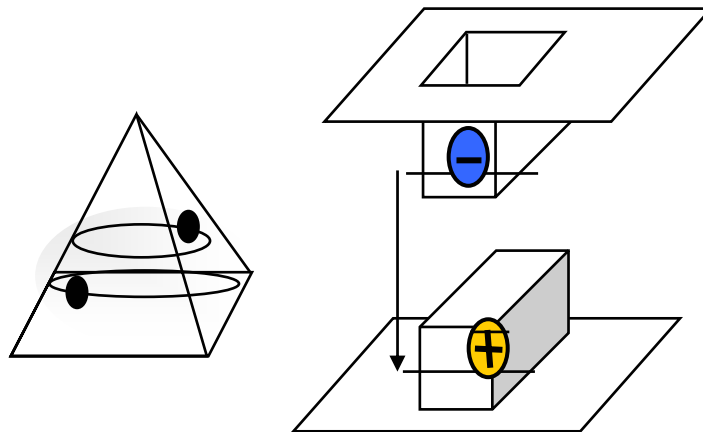
Fig. 3.5. SEM bird's-eye-view and cross-sectional view of InGaN QD structures.
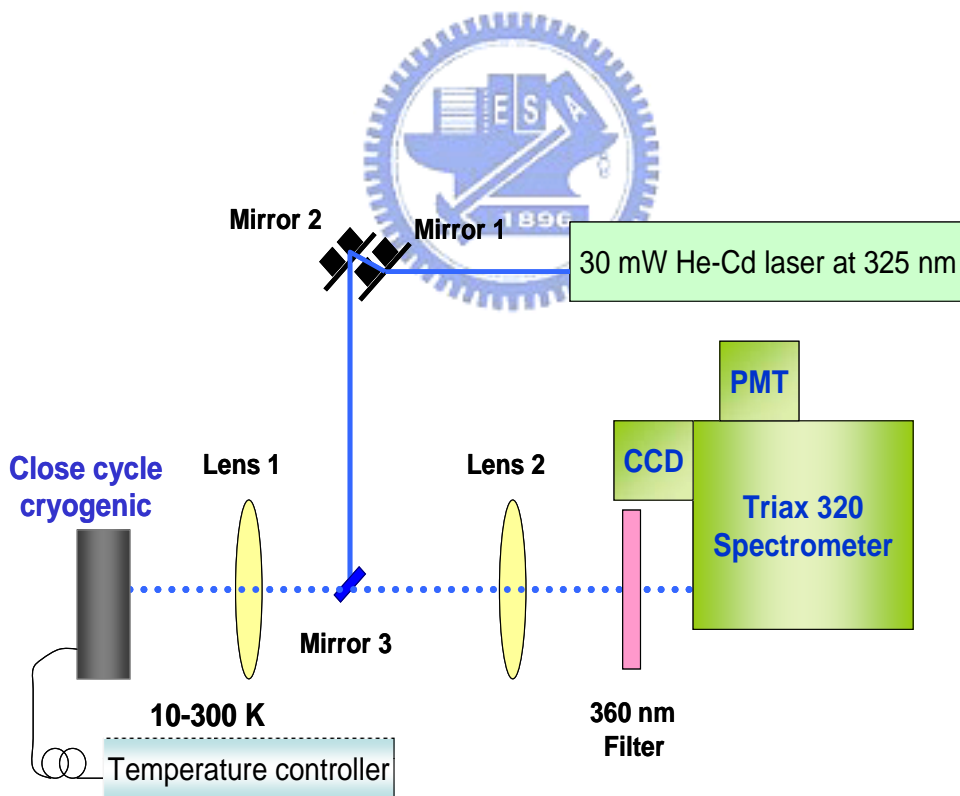
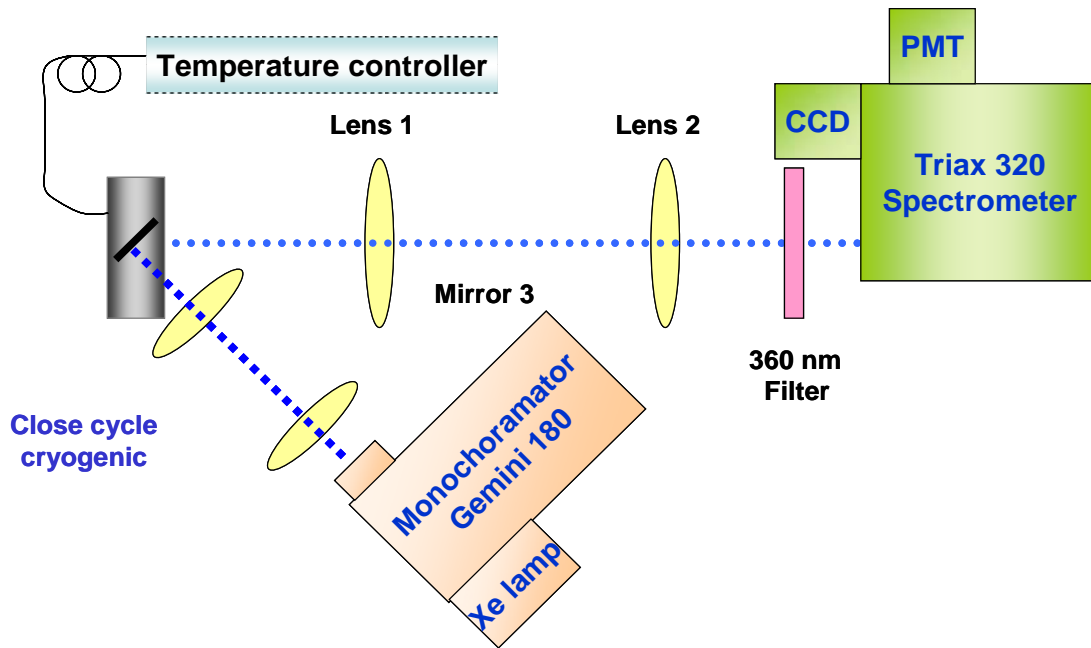Fig. 3.6. Setup diagram of the He-Cd photoluminescence measurement system.

Fig. 3.7.   Setup diagram of the photoluminescence excitation measurement.
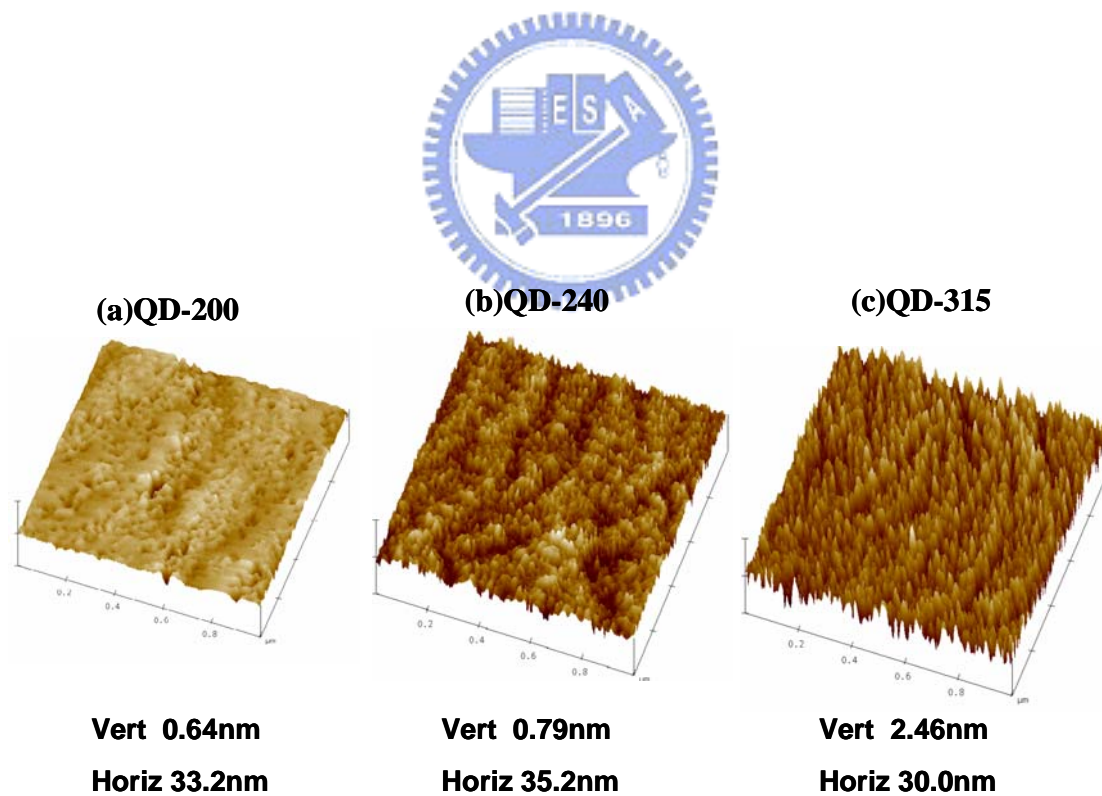

(a)QD-200   **(b)QD-240**   **(c)QD-315**

Vert 0.64nm   **Vert 0.79nm**   **Vert 2.46nm**

Horiz 33.2nm   **Horiz 35.2nm**   **Horiz 30.0nm**

Fig. 3.8.   1μm × 1μm AFM images of samples QD-200, QD-240 and QD-315.
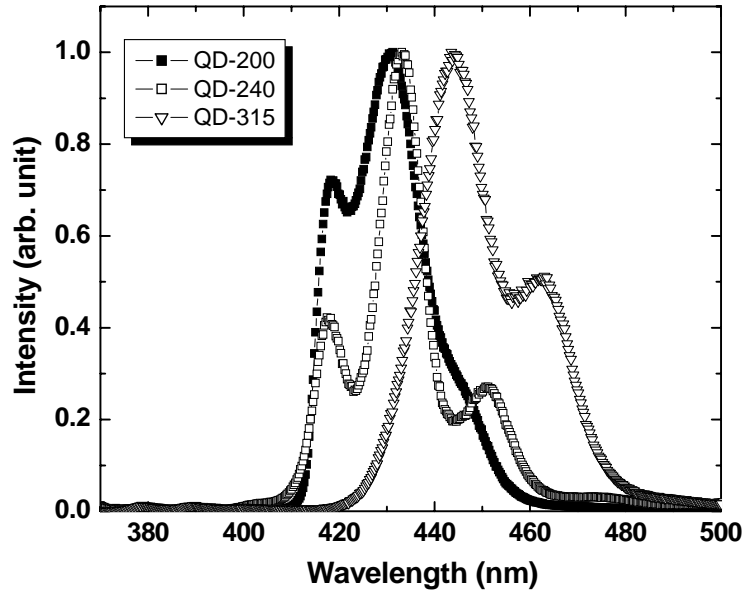
Fig. 3.9. Normalized PL spectra for QD-200, Qd-240 and QD-315 at 10K.
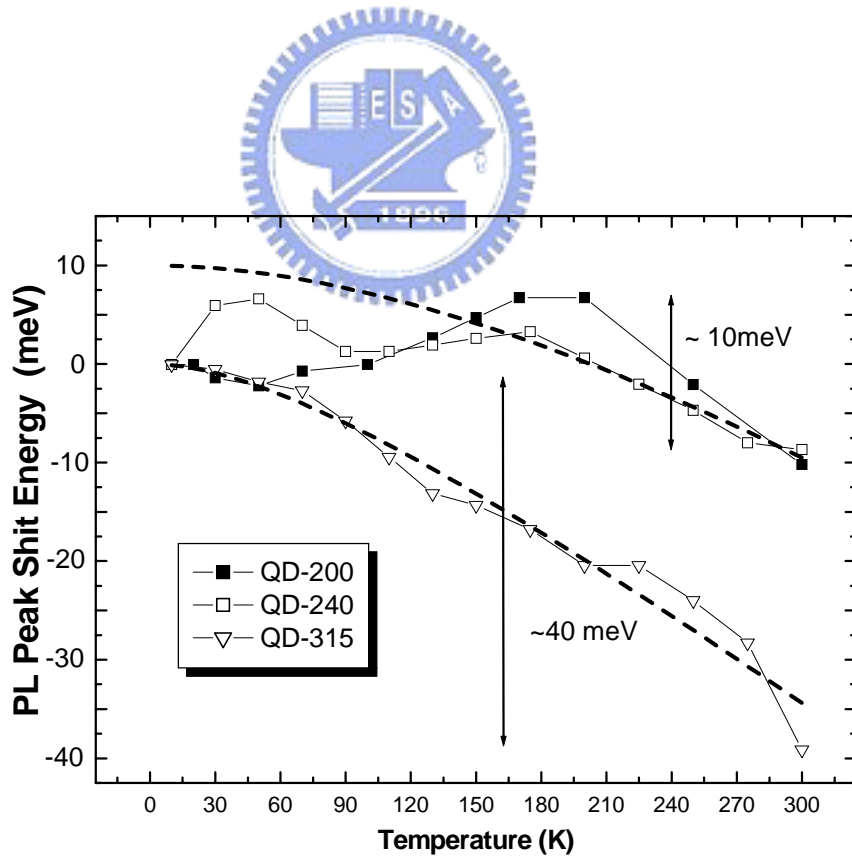

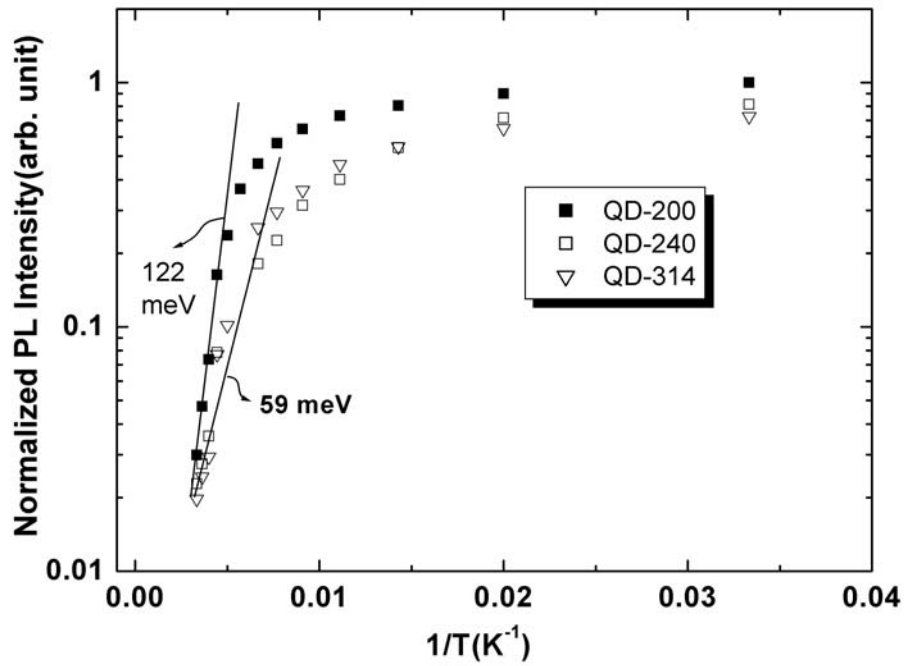Fig. 3.10. The PL peak shift energy for samples of QD-200, QD-240 and QD-315.

Fig. 3.11. Arrhenius plot of normalized PL intensity as a function of temperature for samples QD-200, 240, 314.
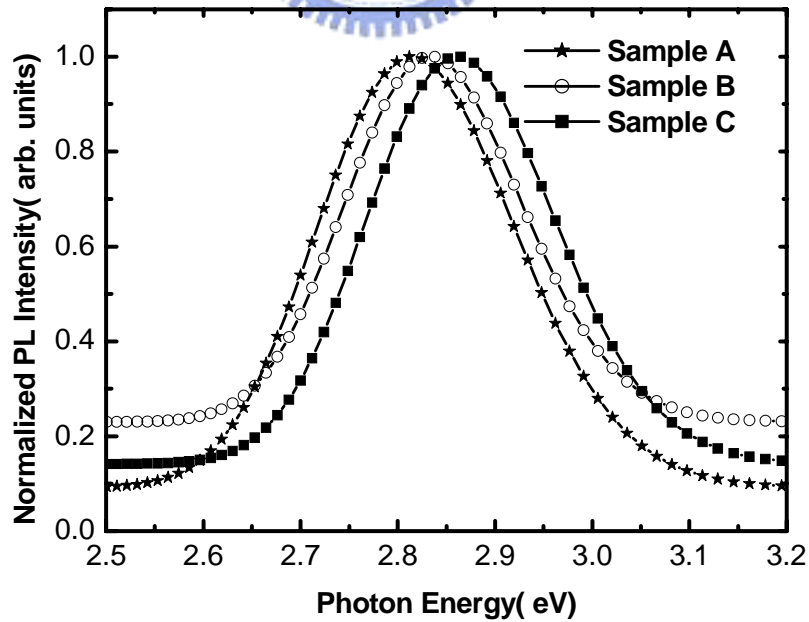

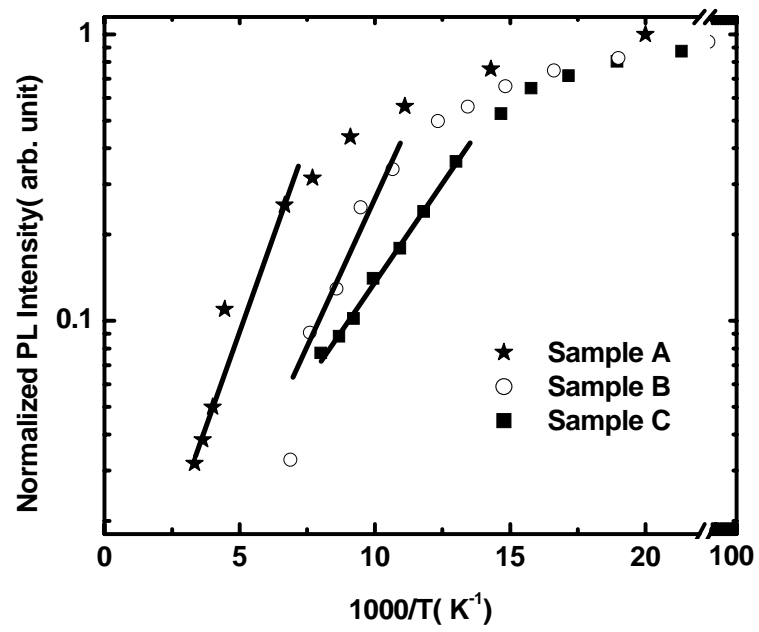Fig. 3.12. Normalized PL spectra from samples A, B, and C at RT.

Fig. 3.13. Arrhenius plots of integrated PL intensity versus the inverse temperature for samples A, B and C.

REFERENCE

[1] Y. Arakawa and H. Sakaki, Appl. Phys. Lett. 40, 939 (1982).

[2] T. Takahahsi and Y. Arakawa, Optoelectron. -Dev. Technol. 3, 155 (1988).

[3] Y. Arakawa, K. Vahala, and A. Yariv, Appl. Phys. Lett. 45, 950 (1984).

[4] T. Takahashi and Y. Arakawa, Nonlinear gain effect in quantum well, wire, and box lasers, 27, 1824 (1991).

[5] Y. Arakawa, IEEE J. Sel. Topics Quantum Electron. 8, 823 (2002).

[6] S. Makino, T. Miyamoto, T. Kageyama, N. Nishiyama, F. Koyama and K. Iga, J. Cryst. Growth 221, 561 (2000).

[7] M. Sopanen, H. P. Xin and C. W. Tu, Appl. Phys. Lett. 76, 994 (2000).

[8] T. Hakkarainen, J. Toivonen, M. Sopanen and H. Lipsanen, Appl. Phys. Lett. 79, 3932 (2001).

[9] K. C. Yew, S. F. Yoon, Z. Z. Sun and S. Z. Wang, J. Cryst. Growth 247, 279 (2003).

[10] M. Herrera, D. Gonzalez, M. Hopkinson, P. Navaretti, M. Gutierrez, H. Y. Liu and R. Garcia, Semicond. Sci. Technol. 19, 813 (2004).

[11] J. Tersoff, Phys. Rev. B 43, 9377 (1991).

[12] W. Sham, W. Walukiewicz, J. W. Ager III, E. E. Haler, J. F. Geisz, D. J. Friedman, J. M. Olson and S. R. Kurtz, Phys. Rev. Lett. 82, 1221 (1999).

[13] M. Kondow, T. Kitatani, S. Nakatsuka, M. C. Larson, K. Nakahara, Y. Yazawa and K. Uomi, IEEE J. Sel. Topics Quantum Electron. 3, 719 (1997).

[14] K. C. Yew, S. F. Yoon and Z. Z. Sun, J. Vac. Sci. Technol. B 21, 2428 (2003).

[15] Y. Masumoto and T. Takagahara, "Semiconductor quantum dots :physics, spectroscopy, and applications," Berlin ;Springer,c2002.New York.

[16] Satoru Tanaka, Sohachi Lwai, and Yoshinobu Aoyagi, Appl. Phys. Lett. 69, 4096 (1996).

[17] Xu-Qiang Shen, Satoru Tanaka, Sohachi Lwai, and Yoshinobu Aoyagi, Appl. Phys. Lett. 72, 344 (1998).

[18] S. Sakai and T. Tatsumi, Phys. Rev. Lett. 71, 4007(1993).

[19] P. Ramvall, P. Riblet, S. Nomura, and Y. Aoyagi, Journal of Appl. Phys. 87, 3883 (2000).

[20] B. Damilano, N. Grandjean, J. Massies, F. Semond, Appl. Surf. Sci. 164, 241 (2000).

[21] S. Chichibu, T. Azuhata, T. Sota, and S. Nakamura, Appl. Phys. Lett. 70, 2822 (1997).

[22] M. Grundmann, J. Christen, N. N. Ledentsov, J. Bohrer, D. Bimberg, S. S. Ruvimov, P. Werner, U. Richter, U. Gosele, J. Heydenreich, V. M. Ustinov, A. Y. Egorov, A. E. Zhukov, and Z. I. Alferov, Phys. Rev. Lett. 74, 4043 (1995).

[23] Y. Narukawa, Y. Kawakami, S. Fujita, S. Fujita, and S. Nakamura, Phys. Rev. B 55, R1938 (1997).

[24] G. Bacher, H. Schweizer, J. Kovac, A. Forchel, H. Nickel, W. Schlapp and R. Losch, Phys. Rev. B 43, 9312 (1991).

[25] H. J. Kim, H. K Na, S. Y. Kwon, H. C. Seo, H. J. Kim Y. Shin, K.H. Lee, D. H. Kim, H. J. Oh, S. Yoon, C. Soneb, Y. Park, E. Yoon, J. Crystal Growth, 269, 95 (2004).

[26] J. F. Girard, C. Dion, P. Desjardins, C. Ni Allen, P. J. Poole, and S. Raymond, Appl. Phys. Lett 84, 3382 (2004).

[27] J. D. Lambkin, D. J. Dunstan, K. P. Homewood, and M. T. Emeny, Appl. Phys. Lett. 57, 1986 (1990).

[28] S. Mackowski, T. Gurung, H. E. Jackson, L. M. Smith, W. Heiss, J. Kossut, and G. Karczewski, Appl. Phys. Lett. 86, 103101 (2005).

[29] S. Malik, C. Roberts, R. Murray, and M. Pate, Appl. Phys. Lett. 71, 1987 (1997).

[30] C. C. Chuo, C. M. Lee, T. E. Nee, and J. I. Chyi, Appl. Phys. Lett. 76, 3902 (2000).

[31] P. G. Eliseev, P. Perlin, J. Lee, and M. Osinski, Appl. Phys. Lett. 71, 569 (1997).

[32] E. C. Le Ru, J. Fack, and R. Murray, Phys. Rev. B 67, 245318 (2003).